An evaluation of several methods of determining the local angle of attack on wind turbine blades

Guntur, Srinivas; Sørensen, Niels N.

Published in:
Journal of Physics: Conference Series (Online)

Link to article, DOI:
10.1088/1742-6596/555/1/012045

Publication date:
2014

Document Version
Publisher's PDF, also known as Version of record

An evaluation of several methods of determining the local angle of attack on wind turbine blades

2014 J. Phys.: Conf. Ser. 555 012045

(http://iopscience.iop.org/1742-6596/555/1/012045)

An evaluation of several methods of determining the local angle of attack on wind turbine blades

S Guntur, N N Sørensen

Wind Energy Division, Technical University of Denmark (DTU), Risø campus, Roskilde, DK

E-mail: srgu@dtu.dk

Abstract. Several methods of determining the angles of attack (AOAs) on wind turbine blades are discussed in this paper. A brief survey of the methods that have been used in the past are presented, and the advantages of each method are discussed relative to their application in the BEM theory. Data from existing as well as new full rotor CFD computations of the MEXICO rotor are used in this analysis. A more accurate estimation of the AOA is possible from 3D full rotor CFD computations, but when working with experimental data, pressure measurements and sectional forces are often the only data available. The aim of this work is to analyse the reliability of some of the simpler methods of estimating the 3D effective AOA compared some of the more rigorous CFD based methods.

1. Introduction

The angle of attack (AOA) of an airfoil is a 2D concept defined as the angle between its chord and the undisturbed streamlines far upstream. A real, finite, airfoil trails vortices which alter the effective angle of attack. Furthermore, if the airfoil is a part of a rotor that adds or extracts energy to/from the flow, additional aerodynamic effects arise making it a challenge to conceptually define the local AOA. The classical BEM theory assumes a 2D behaviour at all span wise positions on the rotor. Although this assumption works quite well in the mid board regions, it breaks down at the tip and the root regions. In fact, here it is also found that the 2D assumptions break down also in mid-board regions, if the span wise load distribution is not uniform. It is necessary to define an effective AOA for the wind turbine blades especially in the root and the tip regions because most aeroelastic codes today use 2D polars to estimate the forces on the rotor blades. Codes based on the classical BEM theory are corrected for the 3D effects near the root region using correction models for rotational lift augmentation, see e.g. [1, 2, 3, 4, 5, 6, 7], and near the tip using correction factors such as Prandtl's, see e.g. [8, 9, 10, 11]. Several methods to estimate the effective AOA on the wind turbine blades exist. In this paper, four of the popular techniques are described and compared using data from existing [12] as well as new full rotor computations of the MEXICO rotor, the details of which are given in the following sections.

2. Methods of determining an angle of attack

Several techniques exist by which the effective AOA can be estimated for a given rotor. Of others, the following four techniques are used in the current work.

1. The inverse BEM method [13, 14], which uses the pre-determined local forces to calculate the local induction.
2. Using CFD data to obtain the annular average of the axial velocity (and thereby the induction $\overline{a}$) at a given radial position in the rotor plane [15, 16, 17].
3. Using CFD data to obtain the the axial velocity at a given radial position in the rotor plane at the location of the blade (a_B). This method is similar to method (2.).
4. Determination of AOA by comparison of high-pressure-side C_P distributions of a 3D case with a 2D case with a known AOA [18].

Methods (1.) and (4.) require sectional force coefficients and pressure distributions, respectively, making them suitable with experimental data where sectional force coefficients and pressure distributions are often the only data available. On the other hand, methods (2.) and (3.) require detailed flow field information upstream and downstream of the rotor, making them more suitable where full rotor CFD data is available.

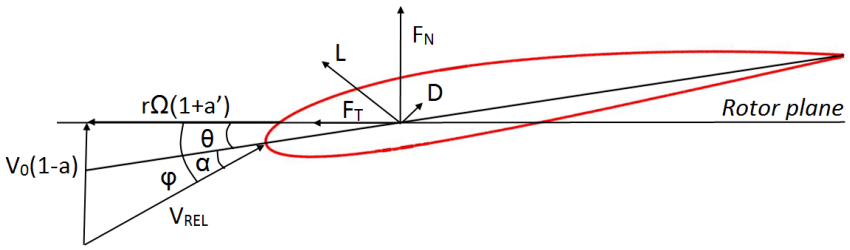

Figure 1. Schematic of a section of a blade with notations employed in this paper.

2.1. Method (1). Inverse BEM method

The inverse BEM methodology, motivated by some previous work [2, 14, 13], utilizes the pre-determined normal and tangential forces on the blades, F_N and F_T, obtained from experiments or CFD computations, to calculate the local induction. Thereby, the local effective AOAs and the 3D lift and drag polars are determined. The inverse BEM algorithm based on the available force coefficients, C_N and C_T, for the MEXICO rotor is summarized below (see e.g., [9, 19] for the classical BEM theory):

(i) Initialize the axial (a) and the tangential (a') induction factors, typically $a = a' = 0$.

(ii) Compute the effective inflow angle ϕ (see figure(1)), as

$$\phi = \tan^{-1}\left[\frac{(1-a)V_o}{(1+a')r\omega}\right] \tag{1}$$

(iii) Obtain sectional C_N and C_T values−in this work, data from full rotor CFD computations of the MEXICO rotor are used.

(iv) Calculate new values of a and a',

$$a_{new} = \frac{1}{\frac{8\pi r F \sin^2\phi}{cBC_N} + 1}, \tag{2}$$

and,

$$a'_{new} = \frac{1}{\frac{8\pi r F \sin\phi\cos\phi}{cBC_T} - 1}. \tag{3}$$

(v) If the difference between the new vales of $[a,\ a']$ and $[a_{new},\ a'_{new}]$ is more than a certain tolerance, go to step 2. Else, continue.

(vi) Compute C_L and C_D as,

$$\begin{aligned} C_{L,3D} &= C_N \cos\phi + C_T \sin\phi, \\ C_{D,3D} &= C_N \sin\phi - C_T \cos\phi. \end{aligned} \tag{4}$$

These values are the new, 3D, lift and drag coefficients.

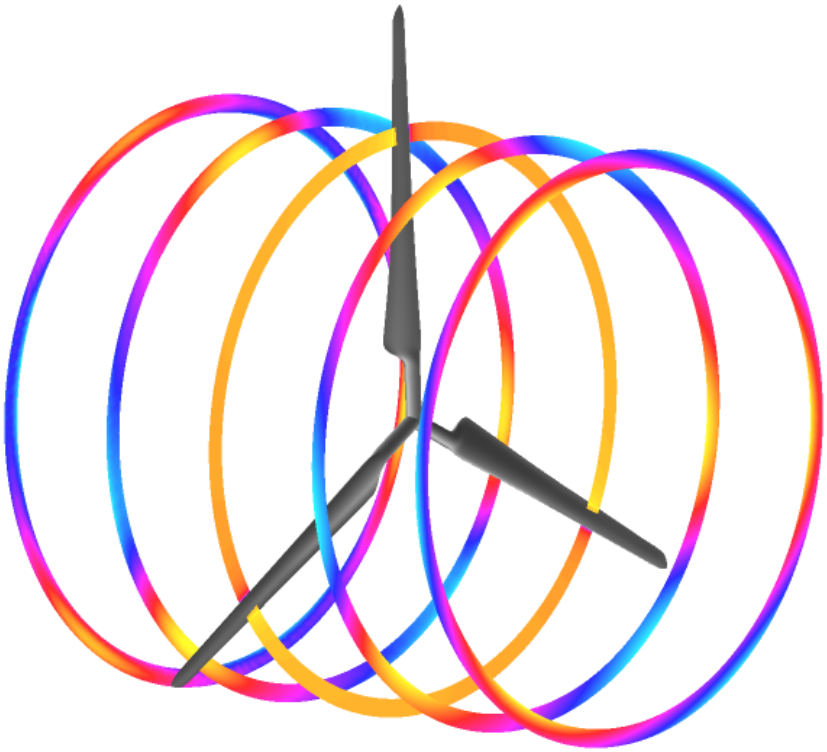

Figure 2. Schematic showing annuli at various stream wise positions over which the axial velocities were extranced and used in methods (2.) and (3.).

2.2. Method (2). Computing the local induced average velocities using CFD

Another method of estimating the local AOA is through the analysis of the velocity field from a full rotor 3D CFD computation. The aim is to obtain the induced axial velocities at the rotor

plane, using the available data at several upstream and downstream locations [15, 16, 17]. The CFD data from [12] was used to obtain the full velocity field in case of the MEXICO rotor. The velocity field within an annulus of a given radial location (see figure (2)) was obtained and averaged, and this procedure was carried out at different stream wise positions to obtain axial velocities as a function of the stream wise position. Once the velocities are known at a set of upstream and downstream positions, its value at the rotor plane can be estimated by interpolation. In this work, this is done using the Lagrangian polynomial interpolation: if there are N points $z = z_i$, $i \in \{1, 2, ...N\}$ at which the value of a function $f(z_i)$ is known, then its value at $z = z_0$ can be determined by the general formula,

$$f(z_0) = \sum_{i=1}^{N} \left[f(z_i) \left(\prod_{j=1, j\neq i}^{N} \frac{z_0 - z_j}{z_i - z_j} \right) \right] \tag{5}$$

The velocities at $z =$ {-1 m, -0.5 m, 0.5 m, 1 m} were obtained from CFD data and the value at $z = 0$ (rotor plane) was estimated using equation (5). A schematic is shown in figure (2) and example in figure (3). Once the velocity is obtained, given the local blade twist and its rotational speed, the local effective AOA can be calculated as

$$\alpha_{eff} = \tan^{-1}\left(\frac{V2}{r\Omega}\right) - \theta, \tag{6}$$

where V2 is obtained as shown in figure (3) and θ is the local twist.

2.3. Method (3). Computing the local induced velocities at the blade using CFD

This procedure is similar to method (2.) described above. Axial velocities at the different points within an annular region shown in figure (2) are extracted from the CFD data. However, in this method, unlike method (2.), the velocities are *not* averaged over the annulus, and as a result the axial velocity is obtained as a function of the azimuth. This is repeated at various locations upstream and downstream of the rotor, as well as at various r/R locations. Interpolation by equation (5) is performed to obtain the axial velocities at the rotor plane. As a result, axial velocity as a function of the azimuth is obtained at the rotor plane for the desired r/R location. As the azimuthal locations of the blades are known, the axial velocity (and thereby the induction) at the blade location is determined, see figure (4) for an example. Once the local velocities are determined, the effective AOA is determined by equation (6).

2.4. Method (4). Determination of AOA through the comparison of 2D and 3D C_P curves

This method is based on the hypothesis that the high-pressure-side C_P distribution of a given airfoil in 3D (rotational) and 2D (stationary) flows subjected to the same AOA, does not change significantly in attached flow [18]. Hence, given a 3D pressure distribution on an airfoil at an unknown AOA, it's closest match to a 2D distribution from a known AOA can be used to estimate the effective AOA in the 3D case. In the current work, the C_P distributions of a set of 2D cases ($0 < \alpha < 20^\circ$) were obtained using 2D CFD computations. Data from the full rotor CFD computations of the MEXICO rotor mentioned previously was used to obtain the 3D C_P distribution at a given radial position (r/R). Thereafter, the pressure side data of the 3D C_P

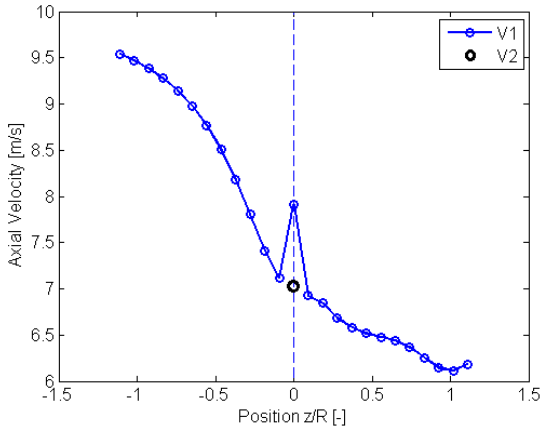

Figure 3. Example - the annular average of axial velocity at span wise position $r/R = 0.25$. The velocities at different stream wise locations obtained directly from the CFD data is denoted by $V1$. $V2$ denotes that obtained from interpolation using equation (5), which is used for estimating the effective AOA. Here, $z/R = 0$ corresponds to the rotor plane and the air flows from left to right.

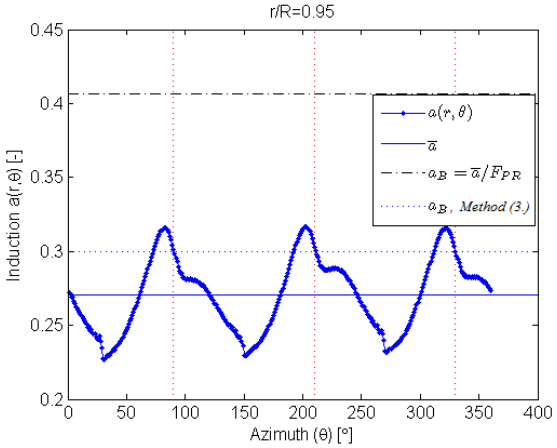

Figure 4. Axial induction factor as a function of the azimuth at $r/R = 0.95$. The blades are located at $\theta = 90°$, $210°$, and $330°$, highlighted by the dotted vertical lines.

curve was isolated and compared with the 2D pressures. The closest 2D match to this 3D C_P distribution was determined, done here using the least squares method, and this angle was taken as the 3D effective AOA. Figure (6) shows an example of the agreement for AOA = 4°.

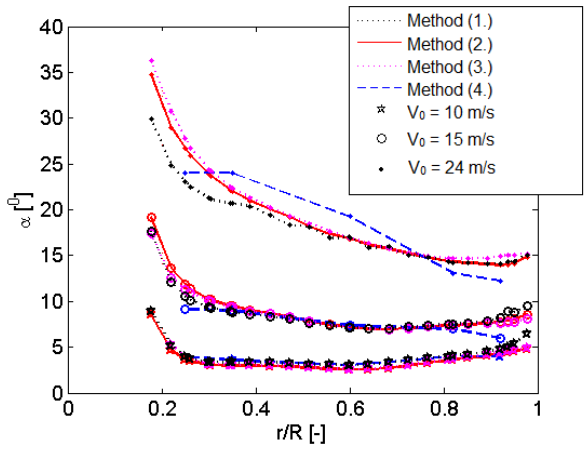

Figure 5. Estimated effective AOAs from the three methods described above.

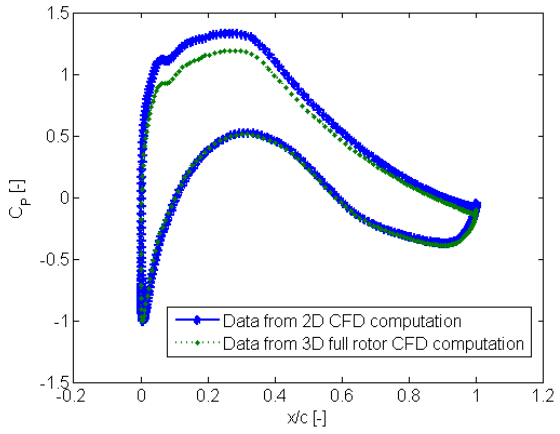

Figure 6. Example - the C_P distribution at a spanwise position $r/R = 0.25$ and $v = 10$ m/s from the full rotor computation, and the C_P distribution from a 2D CFD computation at AOA = 4°.

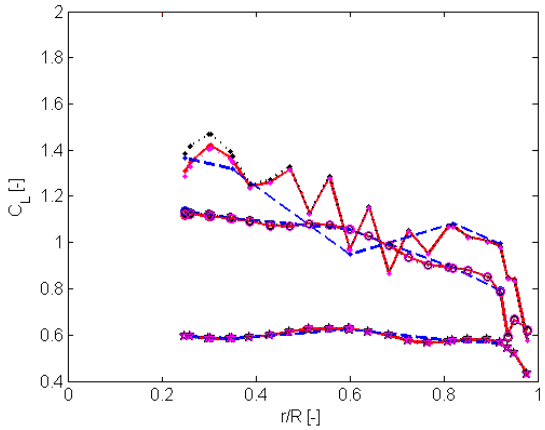

Figure 7. Estimated C_L values using the effective AOAs from figure (5).

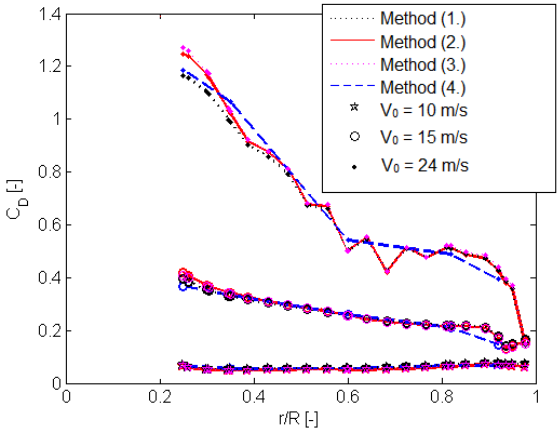

Figure 8. Estimated C_D values using the effective AOAs from figure (5).

3. The MEXICO experiment

The MEXICO (Model Experiments in Controlled Conditions) experiment was a project that was partially funded by the European commission and was conducted in 2006 in the large scale facility of the DNW (German-Dutch) wind tunnel in the Netherlands [20]. This experiment generated, among other signals, surface pressure data on the blades of a wind turbine rotor of 4.5 m diameter that can be used to extract the forces on the blades. In the experiment, pressure distributions at five span wise positions were measured, at several pitch settings and for three tip speed ratios. The combination of these parameters gives rise to various effective AOAs at different positions on the blade. Full rotor CFD simulations of the MEXICO rotor have been carried out for the same operating conditions previously [12]. The current work includes the data from [12] as well as some new computations, which are described in the later sections. The original MEXICO database consists of many different cases, like yaw, different pitch angles, dynamic tests, etc., but here the focus is on those cases with steady inflow, zero yaw, fixed pitch angle ($-2.30°$), rotor speed $\omega = 425$ rpm, and free stream wind speeds $V_0 = \{10, 12, 15, 17, 21, 24, 28\}$ m/s.

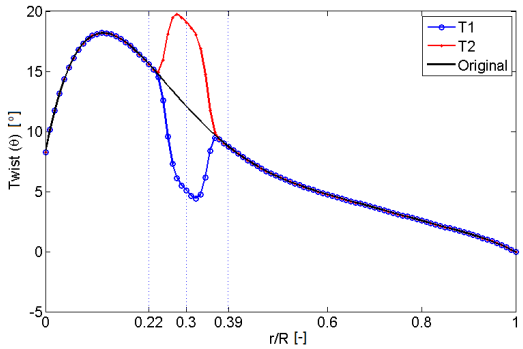

Figure 9. Modified twist distributions of the rotor, $T1$ and $T2$.

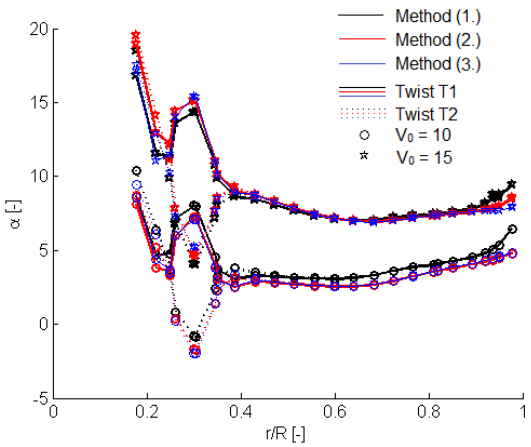

Figure 10. Angle of attack as a function of r/R, for twisted cases $T1$ and $T2$.

4. CFD computations

The CFD computations of the MEXICO rotor were performed with the Ellipsys3D CFD solver, as described in the work of Bechmann *et al.*, see [12]. In addition, in order to investigate the possible effects of a trailing vortex in the mid-board regions, new computations of a re-twisted MEXICO rotor have been carried out. The only difference between the rotor configuration in [12] and the new computations is the new blade twist distribution, which is shown in figure (9) as $T1$ and $T2$. These new computations were carried out at $V_0 = \{10, 12, 15, 17, 20, 25\}$ m/s.

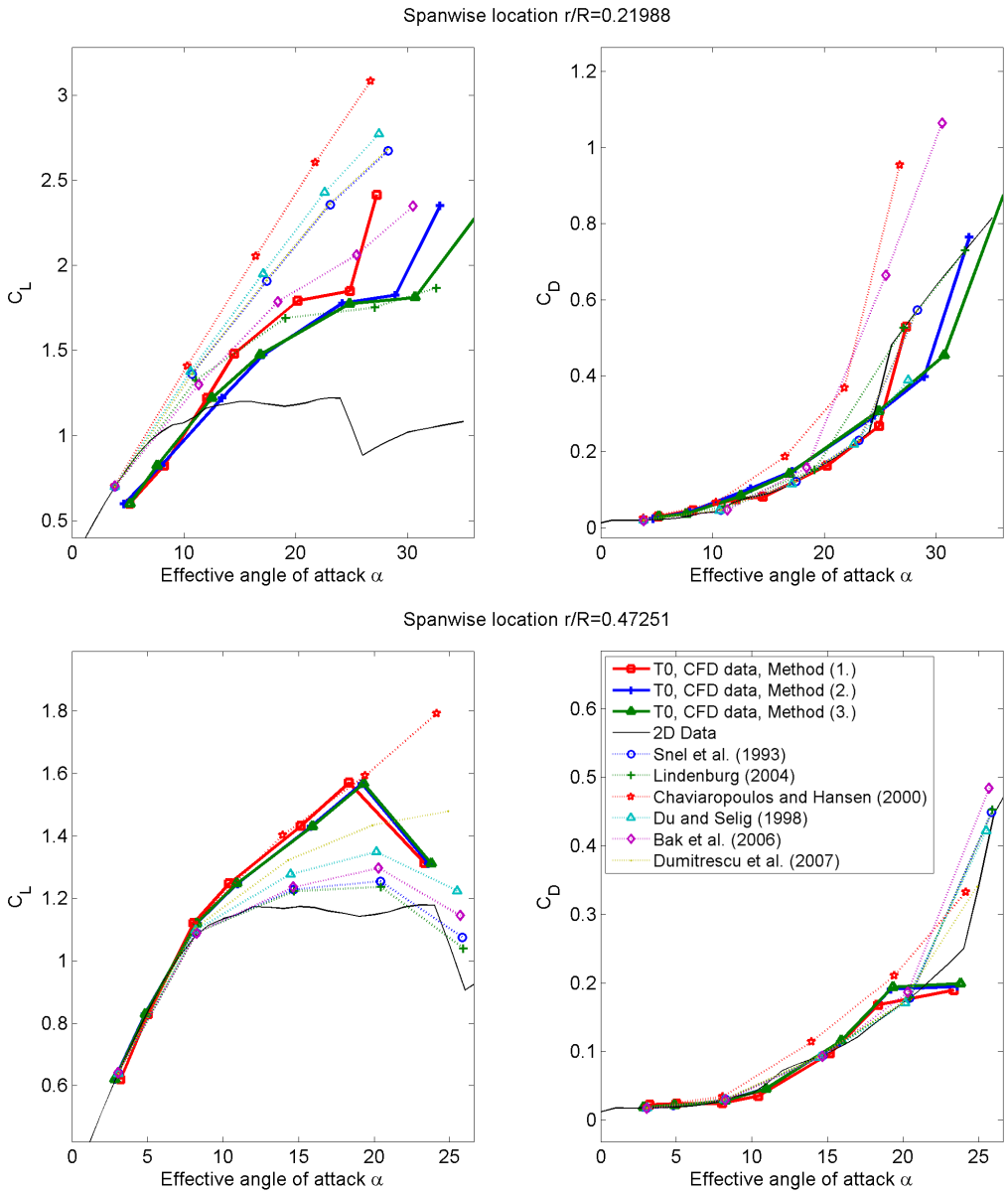

Figure 11. A comparison between the lift and drag polars as predicted by the 3D correction models and CFD data at $r/R \simeq 0.22$ and 0.47. The 2D data is taken from wind tunnel experimental data at $\mathrm{Re} = 0.5 \times 10^6$, interpolated linearly to obtain the estimates at the desired AOAs and r/R locations.

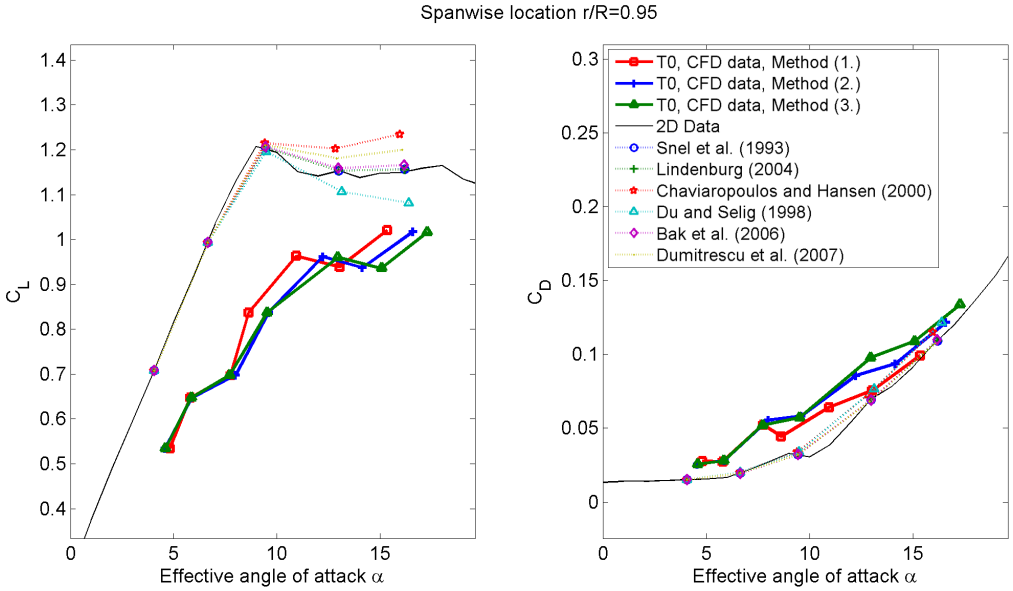

Figure 12. A comparison between the lift and drag polars as predicted by the 3D correction models and CFD data at $r/R \simeq 0.95$. The 2D data is taken from wind tunnel experimental data at $\mathrm{Re} = 0.5 \times 10^6$, interpolated linearly to obtain the estimates at the desired AOAs and r/R locations.

5. Results and discussion

The methods (1.) to (4.) were applied to the data from CFD computations of the MEXICO rotor, and the following observations have been made.

Figures (5), (7) and (8) show the effective AOA, 3D force coefficients C_L and C_D respectively for the original MEXICO rotor as a function of the span wise position, for cases $V_0 = \{10, 15, 24\}$ m/s. As one would expect, in the low and medium wind speed cases $v = 10$ and 15 m/s, there is good agreement in the AOA, C_L and C_D between methods (1.) to (4.) in the mid-board region.

In the case of $v = 24$ m/s, the effective AOAs are in the range of approximately $15° - 25°$, at which angles the airfoils on the blades are fully stalled. Consider the $v = 24$ m/s case in figure (5). It can be seen that method (4.) deviates significantly relative to the other methods. As described earlier, in method (4.), given a 3D pressure distribution, a closest 2D match is searched for. It has been observed here that at high AOAs the change in the C_P distribution in the 2D case (on the high-pressure-side) between consecutive AOAs is insignificant, and so there are some cases where a unique match between the 3D and the 2D distributions cannot be obtained. It is due to this reason that method (4.) fails as the airfoil begins to experience separation. Therefore, since it not known a priori whether the airfoil is operating in separated flow, method (4.) is considered to be unreliable for the current analysis and will be ignored henceforth.

Figures (11) and (12) show polars extracted from the CFD computations along the blades, as well as the estimates by different 3D correction models for inboard lift augmentation applied to a classical BEM code. The airfoil data used in this BEM code are 2D wind tunnel experimental data from the MEXICO database. The MEXICO rotor blades consist of three different airfoil sections of known geometry and polars, connected by transition regions. To estimate the polars in the transition regions, linear interpolation based on the nearest known airfoils was performed.

From figure (11), it can be seen that the methods (1.), (2.) and (3.) are in reasonable agreement for small AOAs. Method (1.) begins to deviate with respect to the other two methods as the AOA increases, and methods (2.) and (3.) remain in very good agreement for relatively higher AOAs. Hence, unless the airfoil operates in deep stall, the performance of methods (2.) and (3.) seems to be nearly the same.

The influence of the tip vortex on the local blade aerodynamics in the tip region and the use of tip loss factors to correct for this effect in BEM codes is well known, see e.g. [8, 9, 10, 11, 19, 21]. The definition of the tip loss factor in terms of the axial induction factor has been a matter of debate. According to [21], its definition by Glauert [9] was

$$\begin{aligned} F_{PR} &= \frac{\overline{a}}{a_B}, \\ \Rightarrow a_B &= \frac{\overline{a}}{F_{PR}}, \end{aligned} \tag{7}$$

where $\overline{a}$ is the annular average of the axial induction at a given radial position (representing infinite blades) and a_B is the local axial induction at the azimuthal blade location for a rotor with finite (in this case, 3) number of blades. Figure (4) shows a comparison between the values of local induction a_B in the tip region estimated directly from CFD, and calculated using equation (7). From this figure, it can be seen that there is a big difference between the value of a_B obtained by method (3.) and that obtained using equation (7). This suggests that the Prandtl's tip correction factor as defined by equation (7) cannot be used to accurately estimate the local velocities at the blade.

Figure (10) shows the AOA estimates along the span wise direction, and figure (12) shows the estimated C_L curves close to the tip, $r/R = 0.95$. From figure (12), it can be seen that the C_L curve is lowered throughout the range of α, which is a result of the tip vortex. Noting that the effect of the trailing tip vortex is to *lower* the lift curve, it is therefore reasonable to expect that a trailing vortex in the mid board section too should have the same effect on the blade sections in its vicinity.

The vortices trailed in case $T1$ have the same orientation with respect to the section at $r/R = 0.30$ as does a tip vortex with respect to the sections near the tip. This implies that its effect on the corresponding airfoil section must be that the estimated lift curve is lowered (compared with the 2D curve), and the opposite in case $T2$. From figure (13) it can be seen that this is indeed the case, as the lift curve is lowered in case $T1$ and increased in case $T2$.

As mentioned previously, a BEM simulation incorporating correction models for the rotational lift augmentation was also carried out. A noteworthy observation is that the augmentation of lift due to rotation ΔC_L $(= C_{L,3D} - C_{L,2D})$ predicted by the 3D correction models is too high in the very inboard sections (see $r/R = 0.22$, figure (11)) and too low in the mid/out board sections (see $r/R = 0.47$, figure (11)), compared to that obtained from CFD. This means that the effect of rotational augmentation occurs for a relatively large portion of the blade, and the rate at which this effect is modelled to change (decrease) as a function of the radial position is in general too high.

6. Conclusion

Various methods of estimating the AOA on wind turbine blades were discussed and their performance was analysed using data from the MEXICO rotor CFD computations. The findings can be summarized as follows:

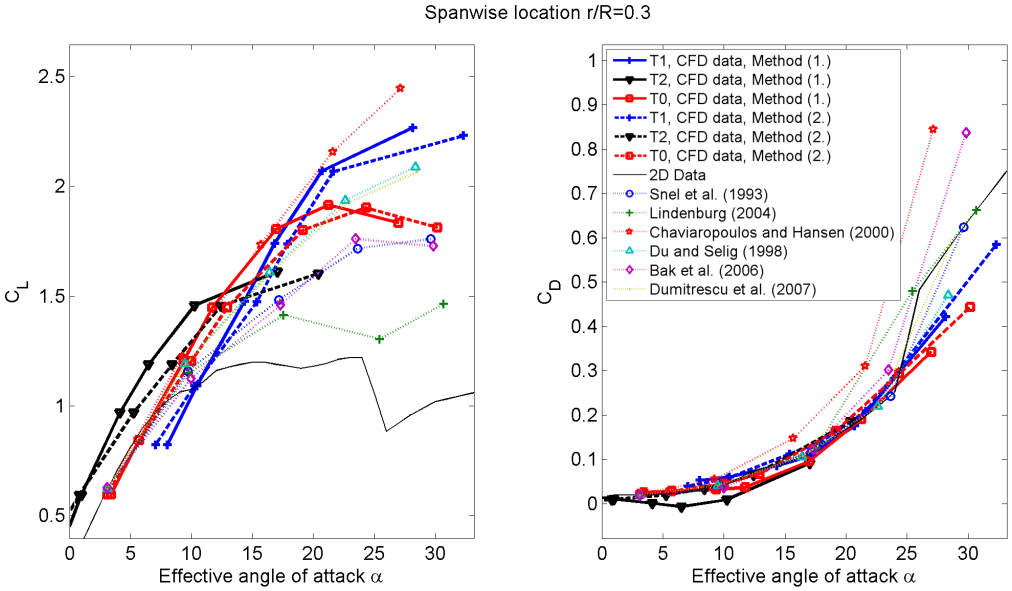

Figure 13. The 3D lift and drag polars computed at $r/R = 0.30$ for the different blade twist configurations $T1$, $T2$, and $T0$, where $T0$ denotes the original MEXICO twist configuration. The 2D data is taken from wind tunnel experimental data at Re $= 0.5 \times 10^6$, interpolated linearly to obtain the estimates at the desired AOAs and r/R locations.

- Overall, method (1.) and the CFD methods ((2.) and (3.)) agree to quite a good degree even near the re-twisted regions in cases $T1$ and $T2$. This means that the inverse BEM method does a reasonably good job.
- As long as the airfoil is not operating in deep stall, methods (2.) and (3.) perform equally well.
- Of the methods studied, method (4.) is the least reliable.
- From the analysis of the additional twist cases $T1$ and $T2$, a discrepancy between the inverse BEM and CFD methods is observed even in the mid-board sections. The dominant mechanism effecting the deviation of airfoil behaviour from 2D is therefore the presence of trailing vortices. Hence, it can be said that the deviation of the force coefficients and the AOA from their classical 2D definition can mainly be attributed to **two** phenomenon:

  (i) rotational augmentation in the in-board sections, and

  (ii) effect due to trailing vortices, at the tip as well as at any given mid board regions where ever there is a non-uniformity in the span wise load distribution.

  A robust correction model for airfoil coefficients should account for both of these effects, which is a potential option for future work.

Acknowledgments

This work is a part of project *SYSWIND*, funded by the European Commission under the framework FP7 programme *Marie Curie*.

References

[1] Bjorck A 1995 Dynamic stall and three-dimensional effects Tech. Rep. EC DXGII Joule II Project No. JOU2-CT93-0345 The aeronautical institute of Sweden
[2] Snel H, Houwink R, Bosschers J, Piers W, van Bussel G and Bruining A 1993 Sectional prediction of 3-D effects for stalled flow on rotating blades and comparison with measurements *Proc. of the European Community Wind Energy Conference* pp 395–399
[3] Chaviaropoulos P and Hansen M 2000 *Journal of Fluids Engineering* **122** 330–336
[4] Breton S, Coton F and Moe G 2008 *Journal of Wind Engineering and Industrial Aerodynamics* **11** 459–482
[5] Bak C, Johansen J and Andersen P 2006 Three-dimensional corrections of airfoil characteristics based on pressure distributions *Proc. of the European Wind Energy Conference* (Athens, Greece)
[6] Lindenburg C 2004 Modeling of rotational augmentation based on engineering considerations and measurements *Proc. of the European Wind Energy Conference* (London, UK)
[7] Du Z and Selig M 1998 A 3-D stall-delay model for horizontal axis wind turbine performance prediction *36th AIAA Aerospace Sciences Meeting and Exhibit* (ASME Wind Energy Symposium, Reno, NV, USA) AIAA-98-0021
[8] Prandtl L 1921 Applications of modern hydrodynamics to aeronautics Tech. Rep. NACA Report No. 116 Gottingen University
[9] Glauert H 1935 *Airplane Propellers* vol IV (New York: Springer) chap Aerodynamic Thoery, pp 169–360
[10] Shen W, Hansen M and Sørensen J 2009 *Wind Energy* **12** 91–98
[11] Branlard E 2011 *Wind turbine tip-loss corrections: Review, implementation and investigation of new models* Master's thesis Technical University of Denmark (DTU)
[12] Bechmann A, Sørensen N and Zahle F 2011 *Wind Energy* **14**(5) 677–689
[13] Lindenburg C 2003 Investigation into rotor blade aerodynamics: Analysis of the stationary measurements on the UAE phase-VI rotor in the NASA-Ames wind tunnel Tech. Rep. ECN-C–03-025 ECN, The Netherlands
[14] Guntur S, Bak C and Sørensen N 2011 Analysis of 3D Stall Models for Wind Turbine Blades Using Data from the MEXICO Experiment *Proc. of the 13th International Conference on Wind Engineering* (Amsterdam, the Netherlands)
[15] Hansen M, Sørensen N, Sørensen J and Mikkelsen J 1997 Extraction of lift, drag and angle of attack from computed 3D viscous flow around a rotating blade *Proc. of the European Wind Energy Conference* (Dublin) pp 499–501
[16] Johansen J and Sørensen N 2004 *Wind Energy* **7** 283–294
[17] Hansen M and Johansen J 2004 *Wind Energy* **7** 343–356
[18] Bak C, Troldborg N and Madsen H 2011 DAN-AERO MW: Measured airfoil characteristics for a MW rotor in atmospheric conditions (Proc. of EWEA)
[19] Hansen M 2000 *Aerodynamics of Wind Turbines* 1st ed (The Cromwell Press, UK)
[20] Snel H, Schepers J and Montgomerie B 2007 The MEXICO project (Model Experiments in Controlled Conditions): The database and first results of data processing and interpretation *Journal of Physics: Conference Series 75*
[21] Shen W, Mikkelsen R and Sørensen J 2005 *Wind Energy* **8** 457–475